# Downloaded from https://www.pnas.org by 173.62.164.145 on May 13, 2025 from IP address 173.62.164.145

# Homologous mutations in human $\beta$ , embryonic, and perinatal muscle myosins have divergent effects on molecular power generation

Chao Liu<sup>a,b,c</sup>, Anastasia Karabina<sup>d,e,f</sup>, Artur Meller<sup>g,h</sup>, Ayan Bhattacharjee<sup>i</sup>, Colby J. Agostino<sup>i</sup>, Greg R. Bowman<sup>i</sup>, Kathleen M. Ruppel<sup>a,b,f</sup>, James A. Spudich<sup>a,b,f</sup> , and Leslie A. Leinwand<sup>d,e,1</sup>

Edited by Edwin Taylor, University of Chicago, Chicago, IL; received September 24, 2023; accepted January 12, 2024

Mutations at a highly conserved homologous residue in three closely related muscle myosins cause three distinct diseases involving muscle defects: R671C in β-cardiac myosin causes hypertrophic cardiomyopathy, R672C and R672H in embryonic skeletal myosin cause Freeman-Sheldon syndrome, and R674Q in perinatal skeletal myosin causes trismus-pseudocamptodactyly syndrome. It is not known whether their effects at the molecular level are similar to one another or correlate with disease phenotype and severity. To this end, we investigated the effects of the homologous mutations on key factors of molecular power production using recombinantly expressed human  $\beta$ , embryonic, and perinatal myosin subfragment-1. We found large effects in the developmental myosins but minimal effects in β myosin, and magnitude of changes correlated partially with clinical severity. The mutations in the developmental myosins dramatically decreased the step size and load-sensitive actin-detachment rate of single molecules measured by optical tweezers, in addition to decreasing overall enzymatic (ATPase) cycle rate. In contrast, the only measured effect of R671C in  $\beta$  myosin was a larger step size. Our measurements of step size and bound times predicted velocities consistent with those measured in an in vitro motility assay. Finally, molecular dynamics simulations predicted that the arginine to cysteine mutation in embryonic, but not  $\beta$ , myosin may reduce pre-powerstroke lever arm priming and ADP pocket opening, providing a possible structural mechanism consistent with the experimental observations. This paper presents direct comparisons of homologous mutations in several different myosin isoforms, whose divergent functional effects are a testament to myosin's highly allosteric nature.

myosins | optical tweezers | molecular dynamics simulation | hypertrophic cardiomyopathy | distal arthrogryposis syndromes

Myosin myopathies refer to a group of skeletal and heart muscle diseases caused by mutations in sarcomeric myosin genes. There are ten such genes in mammals, and mutations in five of them have been linked to disease (1, 2). These diseases are usually autosomal dominant and are largely the result of missense mutations. Some are relatively common, such as hypertrophic cardiomyopathy (HCM) that occurs in ~1 in 500 people (3) to 1 in 200 people (4), while others are rare such as Freeman-Sheldon syndrome (FSS) (5). They can be associated with a risk of sudden death as is the case with HCM, or not be associated with reduced lifespan but have profound effects on quality of life. Despite high sequence conservation among members of the sarcomeric myosin family, they exhibit biochemical and biophysical functional diversity (6) and play distinct roles in heart and skeletal muscles (7–9).

In the current study, we evaluated the functional effects of mutations of the same highly conserved arginine residue in the motor domain of three different myosin genes that cause three distinct diseases (Fig. 1). The mutations are R671C in MYH7 that causes HCM (10), R672C and R672H in MYH3 that cause FSS (11), and R674Q in MYH8 that causes trismus-pseudocamptodactyly syndrome (TPS) (12-14). The highly conserved R671 residue is located inside the myosin head between the active site and the lever arm (Fig. 1A). It resides on the third  $\beta$ -strand and likely interacts with residues of the relay helix, SH1–SH2 domain, and adjacent β-strands (15), regions that undergo major conformational changes during the myosin ATPase cycle (16). Thus, mutations of this residue are expected to have consequential disruptions of myosin's mechanoenzyme activity in all three isoforms.

The MYH7 gene is expressed in the heart and slow skeletal muscle in humans while MYH3 and MYH8, otherwise known as embryonic and perinatal, are expressed transiently in fetal developing skeletal muscle (17, 18). The clinical features of HCM are a hypertrophied hypercontractile heart with increased risks of atrial fibrillation, heart failure, and sudden cardiac death (19). Thousands of mutations across the genes encoding proteins

# **Significance**

Heart disease is the leading cause of death worldwide, and its most common inherited form is hypertrophic cardiomyopathy, a disease of the heart muscle affecting over 1 in 200 people. In comparison, diseases involving congenital skeletal muscle contractures such as Freeman-Sheldon syndrome and trismuspseudocamptodactyly syndrome are rare but still have devastating effects on quality of life. All three can be caused by various mutations in myosins, the motor protein responsible for muscle contraction. Interestingly, there is one particular position that, when mutated in three different myosins, causes these three distinct diseases. Using a multitude of biochemical, biophysical, and computational approaches, we uncover the divergent molecular effects of the mutations to provide understandings of both disease mechanisms and protein allostery.

Competing interest statement: J.A.S. is cofounder and on the Scientific Advisory Board of Cytokinetics, Inc., a company developing small molecule therapeutics for treatment of HCM. J.A.S. is cofounder and CEO, and K.M.R. is cofounder and Research and Clinical Advisor, of Kainomyx, Inc., a company developing small molecule therapeutics targeting myosins in parasites. G.R.B. is cofounder and equity holder in Decrypt Biomedicine.

This article is a PNAS Direct Submission.

Copyright © 2024 the Author(s). Published by PNAS. This article is distributed under Creative Commons Attribution-NonCommercial-NoDerivatives License 4.0

<sup>1</sup>To whom correspondence may be addressed. Email: leslie.leinwand@colorado.edu.

This article contains supporting information online at https://www.pnas.org/lookup/suppl/doi:10.1073/pnas. 2315472121/-/DCSupplemental.

Published February 20, 2024

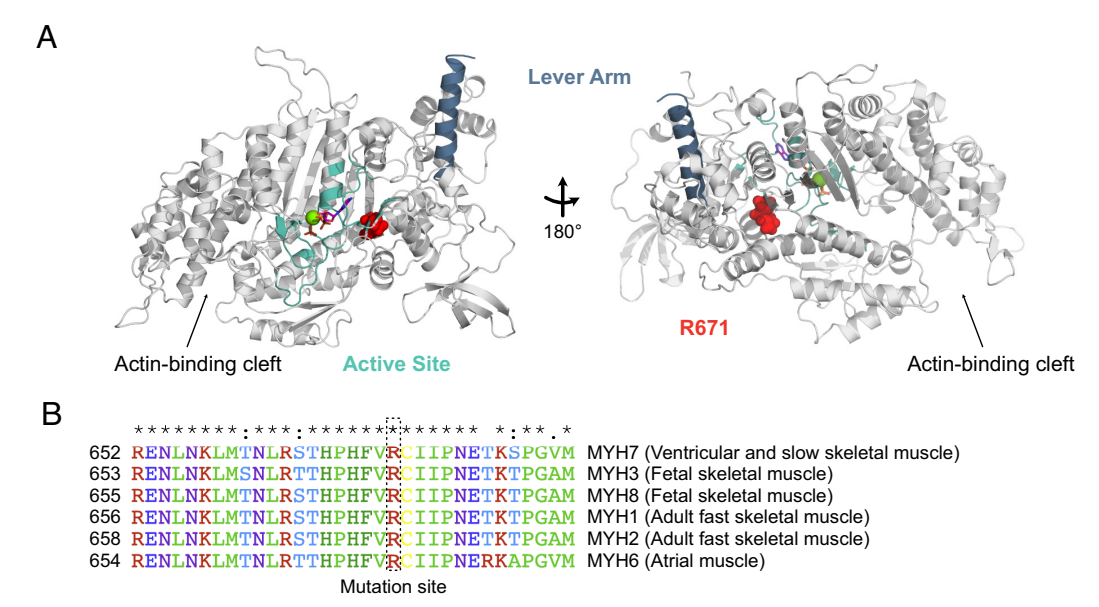


Fig. 1. Mutations at a highly conserved location in the motor domain of different myosin isoforms cause distinct diseases. (A) A homology model structure of β-cardiac myosin motor domain (template PDB 5N6A/5N69, see Materials and Methods) highlights that the arginine residue (R671) is located between the active site and lever arm. (B) A multiple sequence alignment of different myosin-lls expressed in various muscles shows that the mutation site is highly conserved. This paper studies homologous R671 mutations in β (MYH7), embryonic (MYH3), and perinatal (MYH8) myosins implicated in HCM, FSS, and TPS, respectively. Sequence identity and similarity are respectively 79% and 89% between β and embryonic myosin, 81% and 90% between β and perinatal myosin, and 85% and 93% between embryonic and perinatal myosin (motor domain with full lever arm).

of the cardiac sarcomere have been identified to cause HCM, with mutations in MYH7 being the second most common (19). Recently, the FDA approved the use of a myosin inhibitor, Mavacamten, for symptomatic obstructive HCM (20). FSS and TPS are congenital muscle contracture syndromes, specifically distal arthrogryposis types 2A and 7 (ref. 21). FSS is characterized by facial contractures ("whistling face"), strabismus, and contractures of the limbs, and is considered the most severe form of distal arthrogryposis (5, 22, 23). Thus far, the only gene implicated in FSS is MYH3, which explains over 90% of cases (11). Trismus pseudocamptodactyly is caused by only one known mutation (R674Q) in MYH8 to date (14). Patients have shortened muscles and tendons and cannot fully open their mouths. Surgery has been used to manage symptoms of FSS and TPS, but no pharmacologic treatments exist.

Until recently, studies to determine the functional effects of disease-causing mutations in striated muscle myosins relied on materials from patient biopsy or animal models. Analysis of patient samples is complicated by the presence of both wild-type (WT) and mutant myosin, along with other myosin isoforms. Racca et al. found that the MYH3 mutation R672C profoundly slowed relaxation in muscle cells and myofibrils isolated from FSS patients (24). They and another study of two other FSS mutations (Y583S and T178I) in Drosophila skinned muscle proposed prolonged actinmyosin bound times as a key mechanism but lacked direct experimental evidence for this hypothesis (25). Analysis of effects of mutations using animal models is complicated by the fact that the mutation resides in a heterologous backbone with significant sequence differences from the human myosin motor (26, 27). Using an R672C Drosophila model, Rao et al. found that heterozygous flies were unable to fly and exhibited severe myofibril disruption progressing to severe muscle degeneration, and R672C myosin isolated from indirect flight muscles of homozygous flies showed no change in the  $k_{cat}$  of the actin-activated ATPase but a 50% decrease in the actin-sliding velocity in an in vitro motility assay (28). Homology modeling suggested that the mutation disrupts communication between the nucleotide-binding site and the lever arm.

Finally, using a recombinant mammalian expression system (6, 29, 30) that overcomes the limitations of the systems described above, Walklate et al. studied the effects of the R672C and R672H mutations on homogeneously purified human embryonic myosin motor domain (subfragment 1, S1) (15). The mutations decreased the  $k_{\rm cat}$  and increased the apparent affinity for actin in the actin-activated ATPase, with a greater effect by the histidine mutation. In transient kinetic studies, the mutant proteins showed significantly decreased ATP hydrolysis rates, increased affinity for actin in the presence of ADP, and decreased ATP-induced detachment rates from actin. R672H also showed enhanced affinity for ADP. Based on a loss of amplitude of the intrinsic tryptophan fluorescence signal in the mutant proteins, the authors hypothesized that the mutations disrupted a key interaction between R672 and F490 on the relay helix to result in improper helix movement during the recovery stroke.

In this report, we extend the analysis of the MYH3 embryonic R672C and R672H mutants to characterization of their biophysical properties at the single-molecule and ensemble levels and compare them to MYH7 β and MYH8 perinatal myosins harboring mutations (R671C and R674Q, respectively) at the homologous residue (Fig. 1). Constructs consisted of human myosin motor domains (β, "βS1"; embryonic, "EmbS1"; perinatal, "PeriS1") recombinantly expressed in mouse myoblast C2C12 cells (9), bound by coexpressed human essential light chain (31) and endogenous mouse regulatory light chain, and with a C-terminal 8-amino acid tag for purification and surface attachment purposes (SI Appendix, Fig. S1). We focus on investigating the three key parameters that determine power production by the molecular motors: overall cycle rate, step size, and load-dependent actin-bound time. Given the sequence conservation of this region of the molecule (Fig. 1), we hypothesized that the properties of the mutant motors would be similar to each other and that the diverse disease phenotypes would be the result of time and tissue distribution differences in the expression of these three myosins. However, as the myosin molecule is highly allosteric, it is not entirely unexpected that our results showed divergent effects in the different isoforms. Further investigation of this allosteric mechanism using molecular dynamics (MD) simulations to compare the same mutation in βS1 (R671C) and EmbS1 (R672C) suggests that differences in pre-powerstroke conformations may account for the experimentally observed differences in motor function.

## Results

Homologous Mutations Had Differential Effects on Myosin ATPase **Activity.** Actin-activated ATP hydrolysis rates were measured in an NADH-coupled solution-based assay, and the data were fit to the Michaelis–Menten model for enzyme kinetics to determine  $k_{\rm cat}$  and  $K_{\rm m}$  of the S1 motors. The WT developmental skeletal motors had a higher ATPase turnover than WT β myosin (Fig. 2 A–E and Table 1) consistent with previous comparisons of human myosin ATPase rates (6, 15, 32) (EmbS1  $k_{\rm cat}$  = 8.8 ± 0.6 s<sup>-1</sup> and PeriS1  $k_{\rm cat}$  = 11.0 ± 4.0 s<sup>-1</sup>, versus βS1  $k_{\rm cat}$  = 4.2 ± 0.8 s<sup>-1</sup>. Mean ± SEM are reported for all measured values throughout this paper. P-values of pairwise comparisons are given in SI Appendix, Table S1). The mutations considerably slowed embryonic and perinatal ATPase rates (R672C EmbS1  $k_{\rm cat}$  = 6.5 ± 0.4 s<sup>-1</sup>, R672H EmbS1  $k_{\rm cat}$  = 4.3 ± 0.3 s<sup>-1</sup>, R674Q PeriS1  $k_{\rm cat}$  = 2.4 ± 0.5 s<sup>-1</sup>). The R671C mutation did not change the ATPase turnover of the β motor ( $k_{\rm cat}$  = 4.9 ± 1.0 s<sup>-1</sup>). This lack of a major effect on ATPase rate is a common trend seen with many HCM-causing mutations in β-cardiac myosin (33).

The apparent affinity of myosin for actin ( $K_{\rm m}$ ) was not significantly changed across WT myosins. However, the  $K_{\rm m}$  was differentially affected by the homologous mutations in the developmental versus  $\beta$  isoforms (Fig. 2F and Table 1). The homologous mutations increased the actin affinity of the developmental myosins but slightly decreased the actin affinity for  $\beta$  myosin.  $\beta$ S1-R671C increased the  $K_{\rm m}$  of the motor by 66%, from 38 ± 7  $\mu$ M ( $\beta$ -WT) to 63 ± 10  $\mu$ M. R674Q-PeriS1 showed the most dramatic effect on  $K_{\rm m}$  with a 17-fold increase in actin affinity (PeriS1 WT  $K_{\rm m}$  = 208 ± 71  $\mu$ M, R674Q  $K_{\rm m}$  = 12 ± 2  $\mu$ M), while the EmbS1 mutations resulted in a ~twofold-threefold increase in actin affinity (WT  $K_{\rm m}$  = 54 ± 15  $\mu$ M, R672C  $K_{\rm m}$  = 28 ± 7  $\mu$ M, R672H  $K_{\rm m}$  = 17 ± 2  $\mu$ M).

Two previous studies, one using *Drosophila* myosin (34) and the other using the same construct as our present paper (15), reported similar trends in steady-state ATPase between EmbS1 and the R672C/H mutations, albeit the latter observed much

more pronounced effects on  $k_{\rm cat}$  and  $K_{\rm m}$  than seen here. That study's use of 0 mM KCl, in comparison to the higher salt concentration (50 mM KCl) used in the present study which would weaken myosin-actin interaction (35), may explain the observed difference in magnitude of effects. Overall, the homologous mutations show a much greater effect on the enzymatic ATPase properties of the developmental skeletal myosin isoforms than on  $\beta$  myosin.

### Homologous Mutations Had Opposite Effects on Motility Velocity.

The WT developmental myosins had significantly higher actinsliding velocity in an unloaded motility assay than  $\beta$  myosin, as expected of the skeletal vs. cardiac isoforms (Fig. 3, Table 1, and Movies S1, S3, and S6). EmbS1 had velocity  $V = 1,473 \pm 28$ mm/s at 23 °C, vs. PeriS1  $V = 1,920 \pm 35$  nm/s. All comparisons of measured parameters hereon are significant unless stated otherwise (e.g. "similar", "not changed"), and *P*-values are given in *SI Appendix*, Table S1. Previously published velocities of the developmental myosins purified from human fetal tissues (36) or from recombinant expression in C2C12 cells (6) are somewhat lower than the values above, likely due in part to their failure to copurify the light chains (6). βS1 had velocity  $V = 837 \pm 5$  nm/s, consistent with values previously published for human β-cardiac myosin (37–44).

The homologous mutations dramatically decreased the actin-sliding velocity of the developmental myosins but slightly increased the velocity of  $\beta$  myosin. R671C increased the velocity of  $\beta$ S1 by 18% (V= 988 ± 15 nm/s at 23 °C) (Fig. 3A, Table 1, and Movie S2). In contrast, R672C and R672H decreased the velocity of EmbS1 by 77% and 88%, respectively (R672C V = 337 ± 5 nm/s, R672H V = 170 ± 2 nm/s at 23 °C) (Fig. 3B, Table 1, and

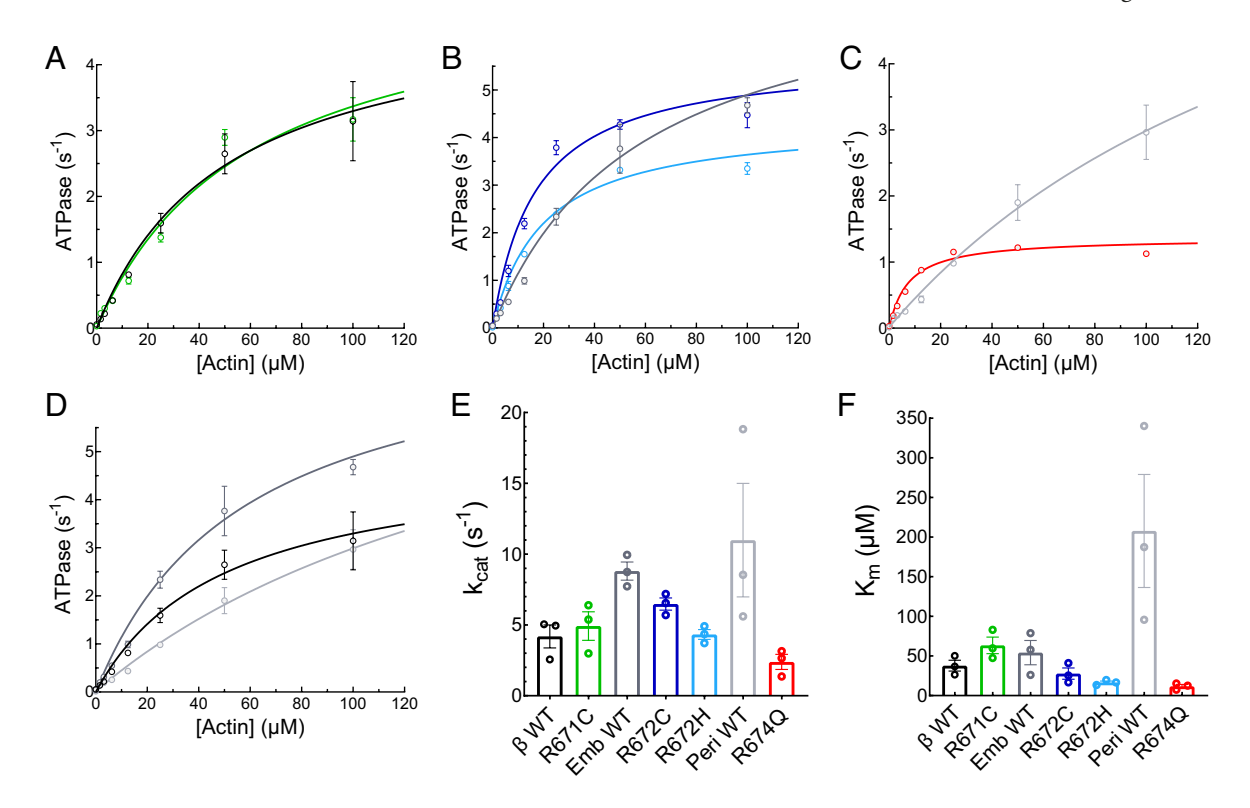


**Fig. 2.** Steady-state actin-activated ATPase rates of myosins measured by solution absorbance. A representative dataset is shown for a single biological replicate of β-WT and R671C (A), EmbWT, R672C, and R672H (B), PeriWT and R674Q (C), with all three WT isoforms shown in (D) where each data point represents the average of three technical replicates at each actin concentration, and error bars represent SD. The data are fit to the Michaelis–Menten equation (solid line) to determine  $k_{\text{cat}}$  and  $K_{\text{m}}$  for each myosin. Three independent experiments, each with their own curve fit, were performed at 30 °C for each protein. Average values of  $k_{\text{cat}}$  (E) and  $K_{\text{m}}$  (F) are plotted as a bar graph with SEM, where data points represent the individual measurements of each independent experiment. The color scheme introduced here is maintained throughout the paper: black, dark gray, and light gray represent the wild types of β, embryonic, and perinatal S1, respectively; green, blue, cyan, and red represent the various mutants as shown.

Table 1. Biochemical and biophysical parameters of myosins

		$k_{\rm cat}$ (s <sup>-1</sup> )	$K_{\rm m}$ ( $\mu$ M)	V <sub>23 °C</sub> (nm/s)	V <sub>30 °C</sub> (nm/s)	$Q_{10}$	$k_0$ (s <sup>-1</sup> )	$\delta$ (nm)	d (nm)	$dr_0$
β	WT	$4.2 \pm 0.8$	38 ± 7	837 ± 5	1,727 ± 15	2.81 ± 0.04	174 ± 6	$0.72 \pm 0.05$	$4.7 \pm 0.4$	0.012 ± 0.002
Embryonic	R671C	$4.9 \pm 1.0$	$63 \pm 10$	988 ± 15	$2,080 \pm 39$	$2.90 \pm 0.10$	$169 \pm 7$	$0.73 \pm 0.03$	$7.0 \pm 0.5$	$0.014 \pm 0.003$
	WT	$8.8 \pm 0.6$	$54 \pm 15$	1,473 ± 28	$3,103 \pm 40$	$2.90 \pm 0.10$	$150 \pm 14$	$0.95 \pm 0.06$	$5.5 \pm 0.3$	$0.028 \pm 0.003$
	R672C	$6.5 \pm 0.4$	$28 \pm 7$	$337 \pm 5$	$759 \pm 3$	$3.19 \pm 0.07$	$74 \pm 5$	$0.37 \pm 0.06$	$2.1 \pm 0.3$	$0.039 \pm 0.004$
Perinatal	R672H	$4.3 \pm 0.3$	17 ± 2	170 ± 2	370 ± 1.3	$3.04 \pm 0.05$	19 ± 2	$0.72 \pm 0.05$	$0.7 \pm 0.3$	0.102 ± 0.012
	WT	$11.0 \pm 4.0$	$208 \pm 71$	1,920 ± 35	$4,065 \pm 20$	$2.92 \pm 0.08$	270 ± 15	$0.76 \pm 0.05$	$7.7 \pm 0.5$	$0.019 \pm 0.007$
	R674Q	$2.4 \pm 0.5$	12 ± 2	$65 \pm 3$	130 ± 2	$2.69 \pm 0.19$	$6.2 \pm 0.4$	$1.24 \pm 0.09$	$0.7 \pm 0.2$	0.195 ± 0.043

ATPase (Michaelis-Menten rate  $k_{cot}$  and constant  $K_m$ , measured at 30 °C), in vitro motility (velocities  $V_{23}$  c and  $V_{30}$  c and temperature coefficient  $Q_{10}$ ), and single molecule optical trapping (actin-detachment rate at zero force  $k_0$ , load sensitivity parameter δ, and step size d, measured at 23 °C). Duty ratio at zero force  $(dr_0)$  and 30 °C is calculated by  $k_{cot}/k_0$ , where  $k_0$  at 30 °C is obtained by correcting the measured 23 °C  $k_0$  with  $Q_{10}$ . Values of measured parameters are mean ± SEM. Uncertainties on calculated parameters  $(Q_{10}$  and  $dr_0)$  are propagated errors. Statistical significance of relevant pairwise comparisons are given in *SI Appendix*, Table S1.

Movies S4 and S5). A previous paper had reported a 50% reduction in motility velocity by R672C in myosin purified from Drosophila (28). R674Q decreased the velocity of PeriS1 by 97% ( $V = 65 \pm 3$ nm/s at 23 °C) (Fig. 3C, Table 1, and Movie S7). The observed significant changes in velocities are direct effects of the mutations on motor function rather than due to altered protein expression or number of inactive heads (SI Appendix, Supplementary text).

To determine whether the mutations alter the temperature sensitivity of myosins and to more closely mimic the physiological temperature, we measured motility velocity at 30 °C in addition to 23 °C. WT  $\beta$ S1 had temperature coefficient  $Q_{10}$  = 2.81 ± 0.04 (error is propagated from calculation of  $Q_{10}$ ) (Fig. 3 D and E and Table 1), consistent with the value measured for human  $\beta$ -cardiac sS1-AC, a construct consisting of the first 808 residues of the myosin heavy chain along with the essential light chain ( $Q_{10}$  =  $3.11 \pm 0.09$ ) (45). WT EmbS1 and WT PeriS1 had similar temperature sensitivities to  $\beta S1$  (EmbS1  $Q_{10}$  = 2.90 ± 0.10, PeriS1  $Q_{10}$  = 2.92 ± 0.08) (Fig. 3 D and E and Table 1). Each homologous mutation had the same relative effect on their respective WT myosin at both 23 °C and 30 °C (Fig. 3 and Table 1). While R672C had a small increase ( $Q_{10} = 3.19 \pm 0.07$ ), the temperature sensitivity was largely invariant in the myosins we studied, independent of isoforms or mutations.

Homologous Mutations Greatly Decreased the Load-Dependent Actin-Detachment Rate of Single Molecules of Embryonic and Perinatal Myosin. Motor function of single myosin molecules was assessed by optical trapping using harmonic force spectroscopy (HFS). In this technique, binding events between a single myosin molecule and an actin filament are measured under different load forces. The sample stage oscillates harmonically so that by the randomness of where myosin initially binds actin, a range of mean forces are automatically applied over the course of many binding events (46) (Fig. 4A). This oscillation at high frequency (200 Hz) also enables the detection of cardiac and skeletal myosins' short millisecond-length binding events under physiological (2 mM) ATP conditions. HFS has been used to measure the load-dependent kinetics and step size of β-cardiac myosin and the effects of numerous cardiomyopathy-causing mutations and myosin activators and inhibitors (42, 44, 47).

Analysis of HFS data is briefly outlined [Materials and Methods, Sung et al., Nat. Commun. 2015 (ref. 46), and Liu et al., NSMB 2018 (ref. 42) for details]. Binding events are automatically selected from the recorded time series of the trapped beads' positions based on a simultaneous increase in oscillation amplitude and decrease in phase relative to the stage position (SI Appendix, Fig. S6). Both criteria occur due to strong coupling between the stage and the trapped beads when myosin binds the actin filament. The duration  $(t_b)$  and mean load force  $(F_0)$  are determined from

each event (Fig. 4B). Durations of events within a force bin are exponentially distributed with a characteristic rate (Fig. 4 B, Inset), the rate of detachment from actin at that load force  $(k_{det})$ .  $k_{det}$  is an exponential function of  $F_0$  (Fig. 4*C*):

$$k_{\rm det}\left(F_0,\Delta F\right) = k_0 I_0 \left(\frac{\Delta F}{k_{\rm B}T}\right) e^{\frac{-F_0\delta}{k_{\rm B}T}}, \qquad [1]$$

where  $k_0$  is the rate at zero load,  $\delta$  is the distance to the transition state of the rate-limiting step in the bound state (a measure of force sensitivity),  $k_{\rm B}$  is the Boltzmann constant, T is temperature, and  $I_0$  is the zeroth-order modified Bessel function of the first kind (to correct for the harmonic force with amplitude  $\Delta F$ ; see Sung et al., Nat. Commun. 2015 (ref. 46) for derivation and SI Appendix, Supplementary Discussion for estimates of its magnitude). Eq. 1 was fitted to the measured rates at different forces to obtain the two parameters  $k_0$  and  $\delta$ . In cardiac and skeletal myosins, ADP release is the rate-limiting step for detachment from actin at saturating (2 mM) ATP concentrations (48, 49), and this step is sensitive to load force (50, 51). Thus, the detachment rate  $k_0$  and its load sensitivity  $\delta$  determined by HFS correspond to the rate of ADP release and its load sensitivity, respectively (51).

WT β and embryonic myosins had similar actin-detachment rates ( $\beta$ S1  $k_0 = 174 \pm 6 \text{ s}^{-1}$ , EmbS1  $k_0 = 150 \pm 14 \text{ s}^{-1}$ ; P = 0.14) (Fig. 4 *D*, *E*, *G*, and *H*, *SI Appendix*, Fig. S7 *A* and *C*, and Table 1), comparable to values previously reported for β-cardiac myosin (42, 44, 46, 52, 53). WT perinatal myosin had significantly faster kinetics ( $k_0 = 270 \pm 15 \text{ s}^{-1}$ ) (Fig. 4 F–H, SI Appendix, Fig. S7F, and Table 1). The force sensitivity of the actin-detachment rate was similar in WT  $\beta$ S1 ( $\delta$  = 0.72  $\pm$  0.05 nm) and PeriS1 ( $\delta$  = 0.76  $\pm$  0.05 nm) (P = 0.63), while that of EmbS1 was slightly higher  $(\delta = 0.95 \pm 0.06 \text{ nm})$  (Fig. 4*I* and Table 1).

R671C did not change the actin-detachment rate of  $\beta$ S1 or its force sensitivity ( $k_0 = 169 \pm 7 \text{ s}^{-1}$ , P = 0.65;  $\delta = 0.73 \pm 0.03 \text{ nm}$ , P = 0.87) (Fig. 4 D and G–I and Table 1). WT and R671C  $\beta$ S1 molecules bound actin for ~6 ms on average under zero load in the exponential distribution of bound times; assistive and resistive load forces up to 4 pN altered the average bound time to ~3 ms and ~15 ms, respectively (SI Appendix, Fig. S7 A and B).

Both R672C and R672H significantly decreased the detachment rate of EmbS1 by 51% and 87% and its force sensitivity by 61% and 24%, respectively (R672C:  $k_0 = 74 \pm 5 \text{ s}^{-1}$ ,  $\delta = 0.37 \pm 100 \text{ s}^{-1}$ 0.06 nm; R672H:  $k_0 = 19 \pm 2 \text{ s}^{-1}$ ,  $\delta = 0.72 \pm 0.05 \text{ nm}$ ) (Fig. 4 E and G-I and Table 1). To put in perspective these rates, R672H molecules bound actin for ~30 ms on average under zero load, compared to ~10 ms for R672C and ~7 ms for WT (SI Appendix, Fig. S7 C–E). R672C's much-reduced force sensitivity is apparent through both the more symmetrical shape of the plot of bound times vs. load force and the shallower slope of the  $k_{der}$  vs load force

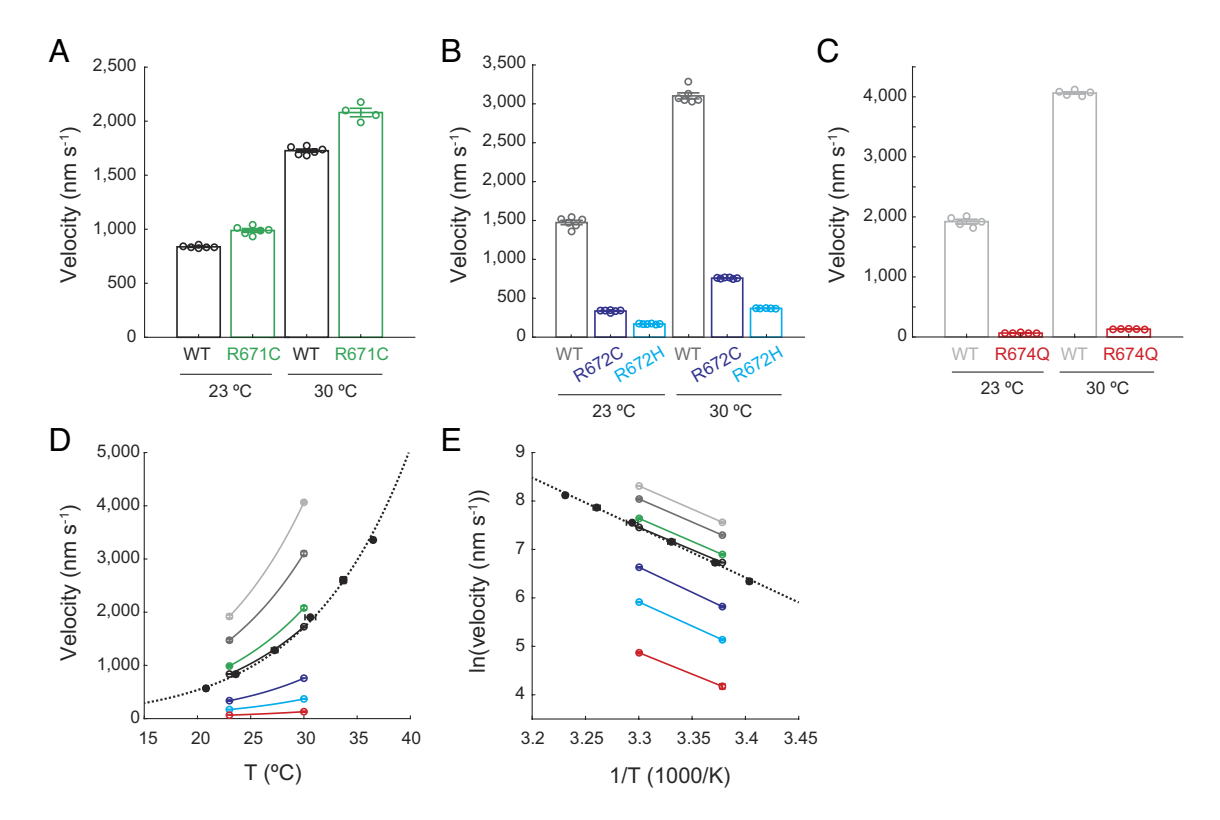


**Fig. 3.** Actin-sliding velocities of myosins measured by the in vitro motility assay. (A–C) Velocities of β S1 WT and R671C (A), embryonic S1 WT, R672C, and R672H (B), and perinatal S1 WT and R674Q (C), each at 23 °C and 30 °C. Reported velocities are "Mean velocities filtered" (see *Materials and Methods* and *SI Appendix*, Figs. S2–S4 for detailed analysis and additional parameters obtained from motility data). Each data point represents one independent experiment. Error bars (most of which are smaller than the lines' thickness) over the bar graph represent mean  $\pm$  SEM. All relevant pairwise comparisons are statistically significant (SI *Appendix*, Table S1). (D) Velocities of each myosin are plotted as a function of temperature. The pairs of data points at 23 °C and 30 °C (open circles) are taken from A–C. The data points spanning ~21 °C to 37 °C (black solid circles) are of WT human  $\beta$ -cardiac short-S1 (residues 1 to 808) as reported in ref. 45. Error bars represent mean  $\pm$  SEM. Solid and dashed lines represent fits to the Arrhenius equation. (E) Data in D displayed as the logarithm of velocity plotted against reciprocal of temperature. All values of velocities and temperature coefficients  $Q_{10}$ 's (from Arrhenius equation fit) are given in Table 1.

relation (*SI Appendix*, Fig. S7D). These single-molecule results of slower detachment rates agree in trend with previously reported stopped-flow solution measurements of the ADP release and ATP binding rates: both R672C and R672H had slower rates than WT EmbS1, with the latter having a larger effect (15).

R674Q dramatically decreased the detachment rate of PeriS1 by 98% while increasing its force sensitivity by 63% ( $k_0$  = 6.2 ± 0.4 s<sup>-1</sup>;  $\delta$  = 1.24 ± 0.09 nm) (Fig. 4 *F–I* and Table 1). While WT PeriS1 molecules bound actin for ~2 to 10 ms on average under different load forces, R674Q molecules stayed bound for ~50 to hundreds of milliseconds (*SI Appendix*, Fig. S7 *F* and *G*).

In summary, while  $\beta$ S1 was not affected by R671C, homologous mutations in EmbS1 and PeriS1 significantly prolonged actin-bound times and altered load sensitivities at the single-molecule level.

Homologous Mutations Had Opposite Effects on Step Size of Single Myosin Molecules. Further analysis of HFS optical trapping data yields the step size of each myosin molecule in addition to its actin detachment kinetics. This analysis adapts the ensemble averaging method (54) to HFS's oscillatory data (44). For each molecule, position traces of all events are aligned at the start of binding, extended to the length of the longest event, and averaged (Fig. 5A). Myosin's stroke is revealed after removal of the oscillations by subtracting a fitted sine function (Fig. 5 A and B).

βS1 had step size  $d = 4.7 \pm 0.4$  nm, consistent with previous measurements in human β-cardiac myosin (44, 53, 55). While EmbS1's step size  $d = 5.5 \pm 0.3$  nm was not significantly different from βS1 (P = 0.088), that of PeriS1 was significantly larger ( $d = 7.7. \pm 0.5$  nm) (Fig. 5 A and B and Table 1).

R671C increased the step size of  $\beta$ S1 by 49% (d = 7.0  $\pm$  0.5 nm). On the contrary, the mutations in the developmental myosins greatly decreased myosin's step size. R672C (d = 2.1  $\pm$  0.3 nm) and R672H (d = 0.7  $\pm$  0.3 nm) decreased the step size of EmbS1 by 62% and 87%, respectively, while R674Q all but eliminated PeriS1's stroke (d = 0.7  $\pm$  0.2 nm) (Fig. 5 A and B and Table 1).

# Actin-Detachment Rate and Step Size of Single Myosin Molecules Explain Effects of Homologous Mutations on Ensemble Motility.

We next investigated the relationship between the single-molecule optical trap and ensemble motility results. Conditions of our motility assay ensured that myosin heads were present in sufficient numbers on the surface and had relatively short tethers such that actin filaments' sliding velocities were predominantly limited by their detachment from myosin rather than attachment (56, 57) (*Materials and Methods*). Under these detachment-limited conditions, velocity can be approximated as the step size divided by the actin-bound time, which is inversely proportional to the detachment rate:  $V = dlt_b = d^*k_{\text{det}}$ . Indeed, velocities were linearly proportional to detachment rates ( $R^2 = 0.81$ ) (Fig. 6A), confirming single-molecule detachment kinetics as the basis of ensemble motility velocity. In contrast, linear regression of velocity versus attachment rate  $k_{\text{attach}}$  (see next section for calculation of  $k_{\text{attach}}$ ) gave  $R^2 = 0.34$  (SI Appendix, Fig. S8).

Consistent with the simple model  $V = d^*k_{\text{det}}$ , differences in the measured detachment rates and step sizes in general accounted for differences in the measured motility velocities (Fig. 6B). The three constructs with the slowest velocities (R674Q PeriS1, R672H EmbS1, and R672C EmbS1) also had the slowest detachment rates and the smallest step sizes, in the same order. WT PeriS1 had

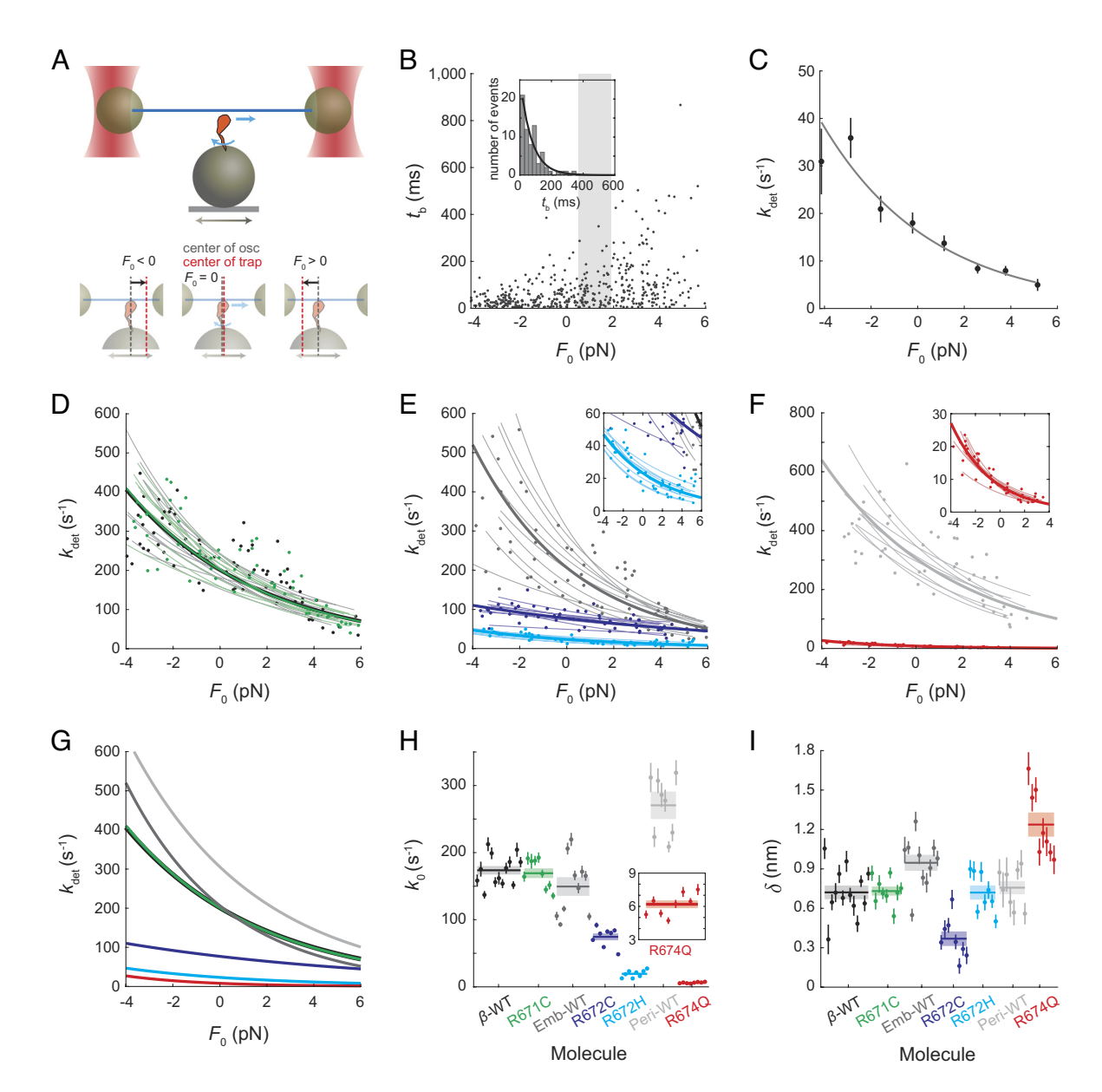


Fig. 4. Single-molecule load-dependent actin-detachment kinetics of myosins measured by optical trapping. (A) Setup of the three-bead system in the optical trap (Top). In HFS, the stage upon which myosin sits oscillates so that a sinusoidal external force with mean  $F_0$  is applied to myosin upon actin binding. Depending on the randomness of when attachment occurs, binding events have different  $F_0$ 's (Bottom).  $F_0 > 0$  represents resistive force, opposite of the direction of stroke, and  $F_0 < 0$  represents assistive force, in the same direction of the stroke. Here, the direction of the lever arm swing and the resulting translation of the actin filament are indicated by the blue curved and straight arrows, respectively. See also SI Appendix, Figs. S5 and S6. (B) All events for one example molecule. Time bound  $t_b$  of each event (obtained as described in SI Appendix, Supplemental Methods and Fig. S6) is plotted against  $F_0$ . Events binned by force (example bin shown as shaded rectangle) have exponentially distributed bound times, from which the detachment rate at that force is determined by maximum likelihood estimation (MLE) (Inset). (C) Detachment rates  $k_{\text{det}}$  determined across all force bins for the example molecule from B. Error bars represent fitting errors from MLE. The force dependent Arrhenius equation with harmonic force correction (Eq. 1) is fitted to the data and yields rate at zero load  $k_0 = 12.5 \pm 0.8 \text{ s}^{-1}$  and force sensitivity  $\delta$  = 0.88 ± 0.08 nm for this example R672H molecule. Errors on  $k_0$  and  $\delta$  of one molecule represent fitting errors. See SI Appendix, Fig. S7 for an example molecule of each protein. (D-F) Load dependent detachment curves of all molecules of β S1 WT and R671C (D), embryonic S1 WT, R672C, and R672H (E), and perinatal S1 WT and R674Q (F). Each thin line represents one molecule. Data points are as described in B and C but displayed without error bars for clarity. Thick curves represent the mean across molecules, also plotted in (G) for comparison. (H and I)  $k_0$  (H) and  $\delta$  (I) for each molecule, each pair of parameters corresponding to one thin line in D-F. Error bars represent fitting errors. Horizontal thick lines represent means of  $k_0$  and  $\delta$  across molecules, which define the thick curves in D-G. Shaded rectangles represent SEM. All values are given in Table 1. All relevant pairwise comparisons are statistically significant except for the following: \$S1 WT vs. R671C  $k_0$  and  $\delta$ ,  $\beta$ S1 WT vs. EmbS1 WT  $k_0$ , and  $\beta$ S1 WT vs PeriS1 WT  $\delta$  (SI Appendix, Table S1). Optical trap experiments were done at 23 °C using 2 mM ATP.

the fastest velocity, consistent with it having the fastest detachment rate and largest step size. As another example, while R671C did not change  $\beta$ S1's detachment kinetics, it did increase the step size, thus explaining the observed increase in velocity (Figs. 3–6).

Measured velocities in the unloaded motility assay were not exactly  $d^*k_0$  (Fig. 6B), as expected given factors involving both model oversimplification and experimental uncertainties. Motility velocities trended higher than  $d^*k_0$ , as reported previously (42, 58). Myosin's nonzero, asymmetrical load dependence  $\delta$  mechanically couples

heads bound to a shared actin filament so that they detach and slide actin faster in ensemble than expected of heads in isolation (58) (SI Appendix, Supplementary text).

**Duty Ratio, Average Force, and Power Predictions.** Duty ratio is the fraction of time that myosin spends in the strongly bound, force-producing state and can be determined given the overall cycle rate  $k_{\rm cat}$  measured by unloaded in-solution ATPase and the actin-detachment rate measured by optical trapping. Since

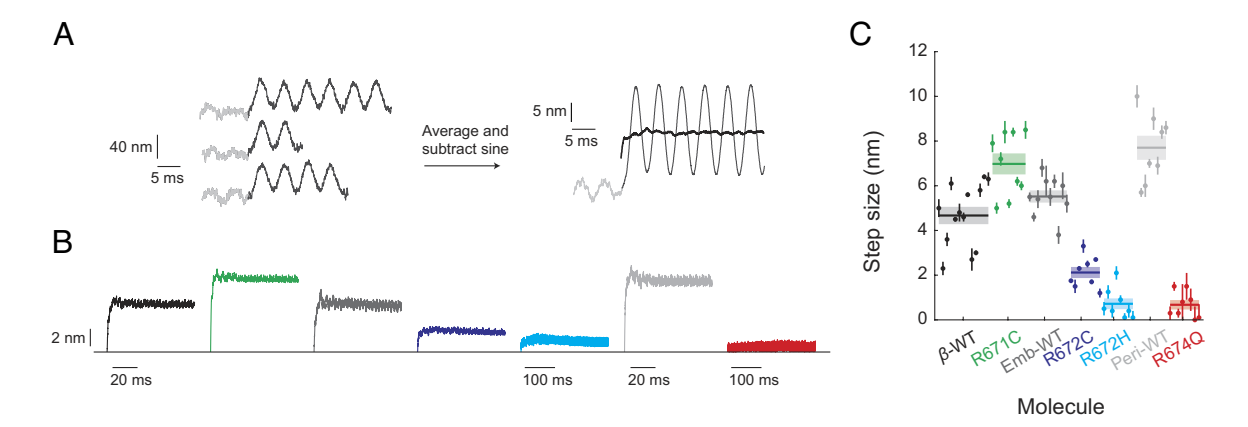


Fig. 5. Single-molecule step sizes of myosins measured by optical trapping. (A) Determination of step size from HFS data. (Left) time traces of three example events before (light gray) and during (dark gray) binding. The amplitude of actin dumbbell oscillations increases upon binding to the myosin which is attached to the oscillating stage (see SI Appendix, Figs. S5 and S6 and Materials and Methods for details of HFS). (Right) hundreds of traces from one molecule are startaligned, extended in time, and averaged (gray). A fitted sinusoid is then subtracted from the averaged trace to reveal the change in actin position due to myosin binding alone (black). (B) Traces of step size from one molecule of each protein studied. (C) Step sizes of all molecules measured. Each data point represents one molecule's step size whose error bars represent uncertainties in the determination of change in actin position. Horizontal lines and shaded rectangles represent mean ± SEM whose values are given in Table 1. All relevant pairwise comparisons are statistically significant except between βS1 WT and EmbS1 WT (SI Appendix, Table S1).

the detachment rate depends on load force, duty ratio is also a function of load force *F*:

$$dr(F) = \frac{k_{\text{attach}}}{k_{\text{attach}} + k_{\text{Jer}}^{-}(F)},$$
 [2]

where  $k_{\text{det}}^{-}(F)$  is the detachment rate calculated without harmonic force correction since we generalize to the non-oscillatory case:

$$k_{\text{det}}^{-}(F) = k_0 e^{\frac{-F\delta}{k_{\text{B}}T}},$$
 [3]

and the attachment rate  $k_{\rm attach}$  was calculated at saturating actin concentrations and assumed to be independent of force:

$$k_{\text{attach}} = \frac{1}{1/k_{\text{cat}} - 1/k_0}.$$
 [4]

We highlight several features of the calculated duty ratios (Fig. 7A and Table 1). First, duty ratio increased as load force increased due to the nonzero load dependence of the detachment rate: myosin remains bound to actin longer under increasing resistive loads. For most of the constructs measured, duty ratio was predicted to more than double as load is increased from 0 to 6 pN. The duty ratio of R672H EmbS1, on the contrary, did not increase to such extent since it was significantly less sensitive to load (Fig. 4I and Table 1). Second, as expected of low duty ratio motors, most of these cardiac and skeletal muscle myosins had duty ratios below 5%, even under high resistive loads. Two exceptions were R672H EmbS1 and R674Q PeriS1 whose duty ratios under zero load ( $dr_0$ ) were 10% and 20%, respectively. This was because their detachment rates were much slower compared to other constructs (Fig. 4H) while their overall cycle rate  $k_{cat}$ (Fig. 2E) were not proportionally lower. Third, we note the effects of mutations. R671C did not change the duty ratio of βS1 (WT  $dr_0 = 0.012 \pm 0.002$ , R671C  $dr_0 = 0.014 \pm 0.003$ ) as it did not affect  $k_{\text{cat}}$  or  $k_{\text{det}}$ . R672C and R672H increased the duty ratio of EmbS1 by 40% and ~3.5×, respectively (WT  $dr_0 = 0.028 \pm 0.003$ , R672C  $dr_0 = 0.039 \pm 0.004$ , R672H  $dr_0 = 0.102 \pm 0.012$ ). R674Q increased the duty ratio of PeriS1 10-fold (WT  $dr_0$  = 0.019 ± 0.007, R672C  $dr_0$  = 0.195 ± 0.043) owing to its dramatically prolonged bound time.

The average force produced by a single myosin molecule is equal to and opposite the load force F averaged over one cycle:

$$F_{av}(F) = F \ dr(F).$$
 [5]

The calculated average forces increased as a function of load because myosin spends more time in the bound, force-producing state (Fig. 7B). Myosins with higher duty ratios (e.g., R672H EmbS1 and R674Q PeriS1) were predicted to produce higher average forces.

Finally, the average power produced by a single myosin molecule is given by the average force  $F_{av}(F)$  multiplied by step size d divided by bound time:

$$P_{\text{av}}(F) = F \ d \ k_{\text{det}}^{-}(F) \ dr(F).$$
 [6]

(Note that Eq. 6 is equivalent to F d  $k_{cat}(F)$ , where  $k_{cat}$  is written here as an explicit function of force because of its detachment rate component). Because step size d is a determinant of power but not duty ratio, trends of the calculated average powers differ from the trends of duty ratios and average forces (Fig. 7C). WT perinatal and embryonic myosins had the highest powers due to a combination of large step sizes and fast kinetics. Despite having the same duty ratio, R671C was predicted to have higher power than WT βS1 due to its larger step size. Finally, all three mutants in the developmental myosins were predicted to cause significantly decreased average power due to a combination of much reduced step sizes and slow kinetics.

Simulations Reveal a Structural Mechanism for Step Size and Detachment Rate Reductions in Embryonic R672C. How does one mutation at a highly conserved homologous site in closely related isoforms lead to such divergent molecular effects on motor function as revealed by our experimental results? As the answer must lie in myosin's highly allosteric nature, we explored this mechanism by using computational modeling and simulations to compare in particular R671C BS1 and R672C EmbS1, the same mutation in the two isoforms.

Given that the R672C mutation caused a reduction in step size and detachment rate in EmbS1 but not in  $\beta$ S1, we reasoned that this mutation must have a different impact on the structural or dynamic properties of the myosin motor depending on its broader sequence context. In most cases, experimental structures of point mutants reveal highly similar structures. On the other hand, a growing body of work supports the view that sequence variation can modulate the probability of adopting different conformations

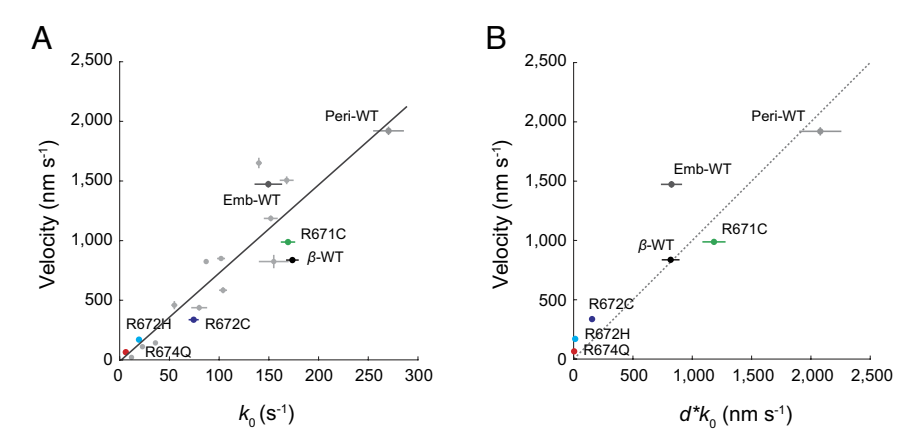


**Fig. 6.** Single-molecule detachment kinetics and step size determine ensemble actin-sliding velocity. (A) Velocities measured in the unloaded motility assay plotted against the detachment rate at zero force  $k_0$  at 23 °C (Table 1). Unlabeled gray data points are from Liu et al., NSMB 2018 (ref. 42). Error bars represent SEM. As velocity is predominantly detachment limited in our motility assay, linear regression gives a slope of 7.4 nm and  $R^2$  = 0.81. (B) Measured velocities V (as in A) plotted against the product of measured step sizes d and measured detachment rates at zero force  $k_0$  (Table 1). Data from Liu et al., NSMB 2018 is not plotted in B because step size data was not available. Horizontal error bars represent propagated errors in calculating  $d^*k_0$ . The dashed line represents  $V = d^*k_0$ .

primed for specific functional roles, even when ground state structures are nearly identical (59–62). When we constructed homology models of R672C EmbS1 and R671C  $\beta$ S1, we found very minor differences between structures. We reasoned, however, that R672C EmbS1 and R671C  $\beta$ S1 would adopt a different set of excited states that could explain their differences in biochemical and biophysical properties. Specifically, we hypothesized that R672C EmbS1 would reduce lever arm priming, reducing its ability to take a productive force-generating step on the actin track.

Hence, we performed MD simulations of R672C EmbS1, WT EmbS1, R671C  $\beta$ S1, and WT  $\beta$ S1 motor domains starting from homology models of fully primed pre-powerstroke crystal structures (PDB: 5N69 and 5N6A) and simulations of WT  $\beta$ S1 starting from a homology model of a post-rigor crystal structure (6FSA). To identify differences in the conformational ensembles of the 4 motors in their pre-powerstroke state, we used a deep learning method known as DiffNets, self-supervised autoencoders capable of identifying features which distinguish ensembles in non-linear ways (63) (SI Appendix, Fig. S9; see Materials and Methods).

We first investigated how the role of the highly conserved arginine residue changes between the post-rigor and pre-powerstroke states. R671 forms a network of hydrogen bonds in the pre-powerstroke state simulations that are significantly more likely than those same hydrogen bonds in the post-rigor state (Fig. 8A). This suggests that R671 stabilizes the pre-powerstroke state and that loss of the hydrogen bonds may destabilize this primed state. Indeed, we observed that mutations to cysteine at this position decrease the angle formed by the lever arm in simulations relative to the experimental post-rigor structure in both EmbS1 and  $\beta$ S1 (Fig. 8B and SI Appendix, Fig. S9C).

However, EmbS1 and  $\beta$ S1 exhibit different behavior at the actin-binding cleft (Fig. 8C and SI Appendix, Fig. S10A). In simulations started from a pre-powerstroke state model where the cleft is initially open, the cleft is more likely to close for R671 βS1 than for R672C EmbS1 (SI Appendix, Fig. S10B). Because cleft closure is necessary for actin binding and a productive power stroke, we compared the position of the lever arm given a closed cleft. We find that among cleft-closed states, while WT EmbS1 and βS1 occupy almost entirely lever-up states (~85°), R672C EmbS1 occupies the lever-down (~50°) states in a majority of simulations (Fig. 8D). This significant loss in lever arm priming likely results in a less productive lever arm swing consistent with R672C's experimentally measured large reduction in step size (Fig. 5). In contrast, while R671C βS1 explores lever-down states with marginally higher propensity WT, it also exhibits a shift to higher-angle lever-up states (Fig. 8D), again consistent with R671C's experimentally measured increase in step size (Fig. 5).

Finally, we find that R672C EmbS1 predominantly occupies conformational states in which the nucleotide-binding site is closed. We measured the opening of the ADP pocket by defining a triangle between the A-loop, P-loop, and Switch I (Fig. 8*E*). While WT EmbS1 has a bimodal distribution of open and closed states (favoring closed), the R672C mutant shows a significant increase in probability density over closed states and a corresponding decrease over open states (Fig. 8*E* and *SI Appendix*, Fig. S11 *A*–*C*). As the release of ADP is a prerequisite for ATP binding and subsequent actin detachment, this finding may explain R672C EmbS1's much reduced actin-detachment rate observed in our single-molecule trapping experiments (Fig. 4*H*).

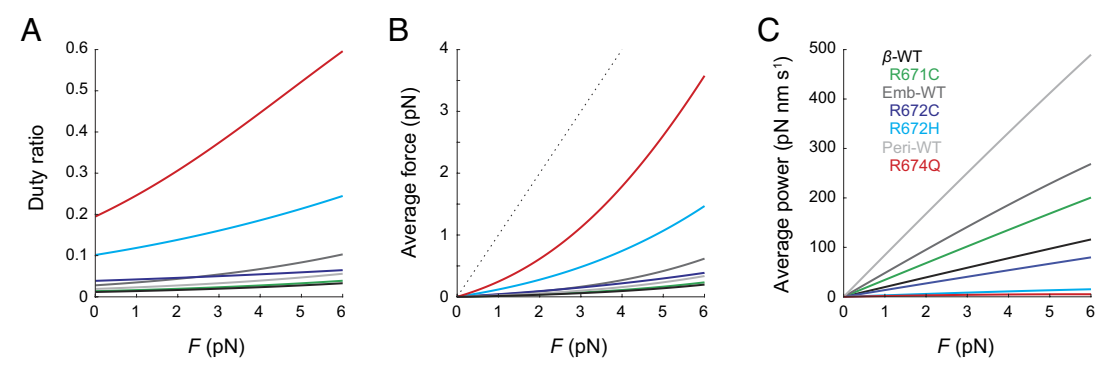


**Fig. 7.** Duty ratio, average force, and average power of myosins determined by ensemble ATPase and single-molecule measurements. (A-C) Duty ratio (A), average force (B), and average power (C) as a function of the load force F, calculated by (Eqs. **2**-**6**). All curves are calculated at 30 °C using values of detachment rate kinetics ( $K_0$ ,  $K_{cat}$ ), step size  $K_0$ ,  $K_{cat}$  and  $K_0$  given in Table 1. The values of duty ratio at zero load are also given in Table 1. The dotted line in  $K_0$  represents the average force if duty ratio = 1, in which case the average force equals the load force.

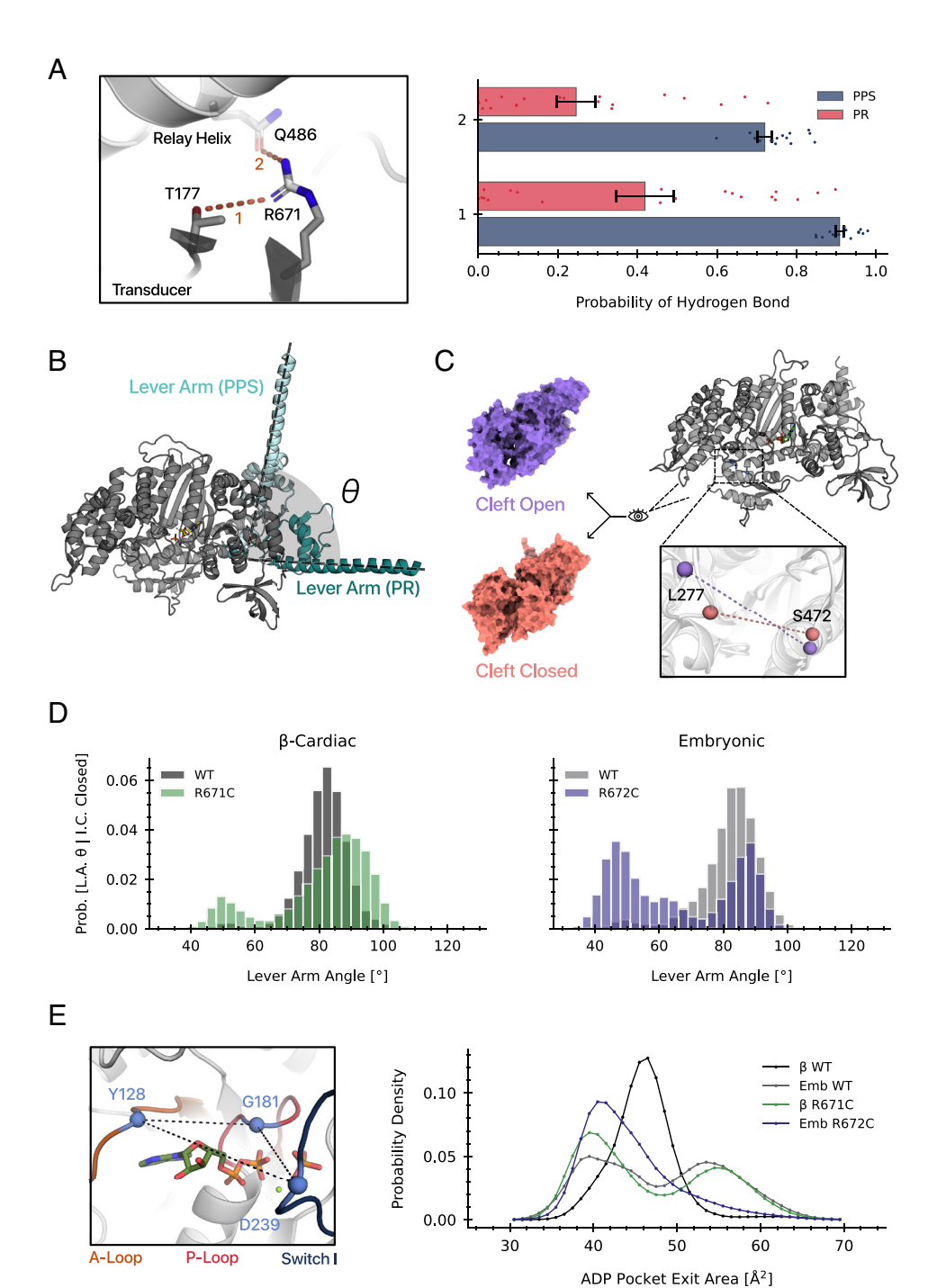


Fig. 8. The R672C mutation reduces lever arm priming and ADP pocket opening in MD simulations of embryonic myosin. All simulations were started from homology models built from template crystal structures of a pre-powerstroke WT β-cardiac myosin. (A) R671's hydrogen bonds selectively stabilize the pre-powerstroke state in β myosin. A representative structure of the two hydrogen bonds is shown on the Left. The bar chart (Right) shows the probability of R671 forming hydrogen bonds with nearby residues T177 (transducer) and Q486 (relay helix) in simulations of the pre-powerstroke and post-rigor states. Data points represent individual trajectories and error bars are SE of the mean obtained from bootstrapping. (B) Schematic depicting the lever arm angle that was measured in structures from simulations. A reference plane was defined by crystal structures of the pre-powerstroke (PDB: 5N69) and post-rigor (PDB: 6FSA) states. (C) Opening and closure of the actin-binding cleft is observed in simulations. The inner cleft distance (64) between the  $\alpha$ -carbon atoms L277 and S472 (MYH7 numbering) is used as a metric of cleft closure. (D) Among cleft closed states, Emb R672C exhibits a population shift toward lever-down states compared to Emb WT. Histograms show the distribution of lever arm angles conditioned on the binding cleft being closed (inner cleft distance ≤11 Å, SI Appendix, Fig. S11D). (E) Emb R672C occupies ADP pocket-closed states more often than Emb WT. The ADP pocket exit area is defined by the area of the triangle formed by the  $\alpha$ -carbon atoms of the three residues in the pocket (Left). Simulations sample both pocket-open and pocket-closed states indicated by two peaks in the histogram (Right).

### **Discussion**

The R671C mutation's lack of effect on several measures of \beta S1 motor function [ATPase (Fig. 1A), actin-detachment rate and force sensitivity (Fig. 4D)] is reminiscent of many [R453C (37); R403Q (39); the converter domain mutations R719W, R723G, and G741R (65); V763M (32); R663H (66)], but not all (the early-onset mutations H251N and D239N (41), previously studied HCM mutations (reviewed in Kawana Front. Physiol. 2022, ref. 33). However, R671C is to date unique in that it increased step size (Fig. 5), whereas previously only unchanged [R453C (37), R403Q (39), D778V, and S782N (47)] or decreased [P710R (44), R712L (67), L781P (47)] step sizes have been reported. Simulations suggest that the larger step size may be the result of a further primed lever arm in the pre-powerstroke state (Fig. 8*D*). This larger step size results in a higher predicted power output

despite an unchanged duty ratio (Fig. 7). Beyond the motor domain, future studies employing an S2-containing construct which enables formation of an autoinhibited state (68, 69) may find that R671C reduces autoinhibition, which, in combination with its increased step size, would form the basis of molecular hypercontractility for this HCM mutation.

In contrast to R671C in βS1, the homologous mutations in the developmental skeletal myosins had much greater effects on all measures of motor function: ATPase (Fig. 1 B and C), actin-detachment rate and its force sensitivity (Fig. 4 E and F), and step size (Fig. 5). The prolonged actin-bound times and reduced step sizes of the embryonic and perinatal mutants are reminiscent, to different degrees, of the investigational heart failure drug omecamtiv mecarbil (OM) (70). OM reduced the actin-detachment rate of  $\beta$ -cardiac myosin by ~10 fold (from ~100  $s^{-1}$  to ~10  $s^{-1}$ ) (42, 53) and demolished its step size (53). Despite these inhibitory effects on the myosin molecule, OM activates the heart muscle through a proposed mechanism in which the prolonged actin-bound times enable myosin heads to cooperatively keep the regulated thin filament open at lower calcium levels, thus prolonging contraction. If so, OM is expected to increase the calcium sensitivity of regulated thin filaments in the motility assay. Future studies may reveal whether the developmental skeletal myosin mutants also have increased calcium sensitivity at the molecular level due to their prolonged actin-bound times.

Comparing myosin motor dynamics provides insight into how the same mutation can have different, or even opposite, effects depending on its sequence context. Predictions based on homology modeling alone (15) would suggest that homologous mutations would have the same effect on motor function. For example, a previous study using homology modeling had suggested that the R671 residue is at a communication hotspot between the nucleotide-binding site and the lever arm, so mutations that perturb this communication would disrupt aspects of force production (28). While our findings of much reduced force sensitivity, actin-detachment rate, and step size in R672C EmbS1 provide experimental evidence for this prediction, the same mutation in  $\beta S1$  (R671C) has a larger step size and no effect on the load-dependent actin detachment kinetics. In MD simulations launched from the same starting structure, R672C EmbS1 is more likely to adopt structures with a closed nucleotidebinding site than R671C βS1. R672C EmbS1 is also more likely to adopt structures with the lever arm in a less primed position when its actin-binding cleft is closed. Thus, MD simulations of each mutant in its specific sequence background are necessary to uncover differences in the distribution of conformations adopted by myosin motors, in order to explain functional differences among homologous mutations (60-62). Future simulation studies will study other homologous mutations for which experimental data exist and incorporate actin, regulated thin filament proteins, etc. to the models to directly probe how myosin behaves when bound to actin.

Our findings of the effects of the mutations at the molecular level provide the mechanisms underlying prior observations in muscle cells. A previous study had found that FSS patient-derived muscle cells and myofibrils containing embryonic myosin bearing the R672C mutation have ~3 to 5× slower rates of relaxation than controls (24). Our results provide direct evidence of slowed actin detachment kinetics at the single-molecule level as the basis for slowed relaxation in cells. MD simulations further provide insight that a smaller ADP exit area may contribute to the longer actin-bound times observed in R672C EmbS1. In another study, FSS mutations (Y583S and T178I) in *Drosophila* skinned muscles increased stiffness by 70 to 77% and decreased power by 50 to 66%, and the authors proposed longer bound times as the underlying mechanism (25). Future optical trapping measurements of these mutants will determine whether that is indeed the case.

More importantly, our results reveal a partial, nuanced correlation between the magnitude of changes due to mutations and disease severity. Within the embryonic isoform, the correlation is clear. The histidine mutation causes a more severe disease than cysteine in FSS patients (22), a trend mirrored by our molecular findings: R672H had larger reductions in ATPase  $k_{\rm cat}$ , actin-detachment rate, and step size than R672C. When comparing across the isoforms, the trend is more nuanced. First, FSS is considered to be the most severe of the distal arthrogryposis syndromes, more so than TPS, but the TPS R674Q mutation in perinatal myosin had the largest effects out of all mutations. Second, in one view, HCM may be considered the most serious of all three myosinopathies because it increases the risk of atrial fibrillation, heart failure, and sudden cardiac death; indeed, it is the leading cause of sudden cardiac death in young athletes (71).

But in a different view, while most patients with FSS and TPS have a normal life expectancy, their clinical signs are arguably much more visually striking than those with HCM. Thus, the HCM R671C mutation's relatively small effect (enhanced step size) in  $\beta$ -cardiac myosin correlates well with an HCM heart's relatively mild phenotype. A mutation in  $\beta$ -cardiac myosin that drastically changes its motor function would be catastrophic in the heart and thus not observed in the population.

Understanding the effects of different mutations on various parameters of motor function enables development of small molecule therapeutics that specifically reverse those changes at the source rather than drugs that act downstream. Prolonged actin-bound times may be a common defect of developmental skeletal myosins implicated in FSS, TPS, and other congenital contractures. In such cases, a logical candidate is 2-deoxy-ATP as it has been shown to increase the actin-detachment rate of single  $\beta$ -cardiac myosin molecules by ~70% (42) and improve muscle contractility (72). There are other small molecule myosin effectors that have been shown to prolong actin-bound times, alter step size, change the overall ATP cycle rate, inhibit actin binding, and/or promote the super-relaxed state (42, 53, 73–75).

While the developmental muscle myosins cease to be expressed in significant levels in almost all skeletal muscles shortly after birth, their devastating effects clearly outlive their transient expression. The significance of longer actin-bound times, altered force sensitivities, and reduced step sizes in the embryonic and perinatal mutants may be appreciated in the context of the critical role of mechanosensation in fetal muscle development (18). The shared defects of dramatically longer bound times and reduced step sizes likely play major roles in disease mechanisms. As both lower (R672C and R672H EmbS1) and higher (R674Q PeriS1) force sensitivities lead to similar diseases involving muscle contractures, the precise mechanism by which altered myosin force sensitivity disrupts development remains to be elucidated in future studies.

In the large myosin superfamily of motor proteins, each isoform has distinct mechanical and kinetic properties tuned to its specific function, as transporters, force sensors, or drivers of muscle contraction. Among muscle myosins, the motor properties of the isoform determine the identity of the particular muscle type (e.g., cardiac, skeletal, smooth). Despite these differences, myosins share a common global structure and perform the same function of actin-based motility through ATP hydrolysis. Perturbations in key conserved regions of the molecule are then expected to be disruptive across isoforms, as is the case for mutations at the homologous R671 residue in β, embryonic, and perinatal myosins. By measuring key factors of molecular power generation, we have found that while each mutation had distinct effects, they affected the developmental myosins much more than  $\beta$  myosin. Furthermore, the observed molecular changes correlate partially with clinical disease severity. MD simulations provide possible structural explanations for the differentially affected properties. Our findings of divergent effects on motor function due to homologous mutations present a striking illustration of myosin's highly allosteric nature and the need to examine mutated forms of the motor using a multitude of experimental approaches in order to understand the molecular mechanisms of such mutations.

### **Materials and Methods**

**Expression and Purification of Proteins.** Recombinant human myosin S1 constructs for MYH7(Met<sup>1</sup>–Ser<sup>842</sup>), MYH3(Met<sup>1</sup>–Ala<sup>844</sup>), MYH8(Met<sup>1</sup>–Leu<sup>842</sup>) containing a GSG-RGSIDTWV C-terminal tag ("affinity clamp", AC) (S1-AC) were cloned into a pUC19 vector, and site directed mutagenesis was performed to generate the four mutations. The transgenes were inserted into pShuttle-CMV of the AdEasy Adenoviral Vector System (Agilent #240009) to produce recombinant

adenovirus. Adenovirus of the seven constructs and the human essential light chain (ELC or MYL3) with a 6×His N-terminal tag (31) was amplified in HEK293 cells and purified from clarified cell lysates in a CsCl step gradient followed by a linear gradient. Recombinant proteins were expressed in adenovirus-infected murine C<sub>2</sub>C<sub>12</sub> myoblasts as described previously (6) and purified through two rounds of affinity chromatography: first using PDZ (76) coupled to Sulfolink™ Coupling Resin (Thermo #20401) to capture the S1 heavy chain by its AC tag, followed by nickel resin to capture the expressed human ELC by its 6×His tag, removing myosin bound to native mouse ELC. Protein used for unloaded motility and optical trap experiments was further subjected to a "deadheading" procedure to remove inactive heads. See Supplementary methods for additional details.

Actin-Activated ATPase. ATPase activity was measured by an NADH-coupled assay (77). Reactions were carried out on a 96-well plate at 30 °C in 200 µL volumes containing 0 to 100  $\mu\text{M}$  actin, 0.2  $\mu\text{M}$  myosin, 20 mM HEPES, 50 mM KCl, 5 mM MgCl<sub>2</sub>, pH 7.5, 5 mM DTT, 3 mM ATP, 3 mM PEP, 1 mM NADH, and 3 to 7 units/mL of pyruvate kinase and lactate dehydrogenase (Sigma P0294). The plate was shaken for 1 min before reading the absorbance at 340 nm every 30 s for 1 h. Statistical significance throughout this paper was determined using two-tailed unequal variances t tests (SI Appendix, Table S1).

In Vitro Motility. Motility measurements used our previously described motility assay (38, 78) with some modifications, using SNAP-PDZ18 to attach the S1-AC to the surface and not using methylcellulose. Multichannel slides were imaged on a 100 × TIRF microscope maintained at 23  $\pm$  0.3 °C or 30  $\pm$  0.3 °C. See Movies S1-S14. Movies were processed by Fast Automated Spud Trekker for filament tracking and velocity analysis (38) (SI Appendix, Figs. S2 and S3). While "Mean velocity - filtered (MVEL<sub>20</sub>)" is reported in Fig. 3, we provide TOP5% MVIS, and %STUCK in SI Appendix, Fig. S4 for comparison. See SI Appendix, Supplementary Methods for additional details.

Single-Molecule Optical Trap Measurements. The load-dependent detachment rates of myosins were measured in a dual-beam optical trap using the HFS method previously described (42, 46, 79) with slight modifications. SNAP-PDZ was used to attach S1-AC to the surface. Step sizes were determined from the same HFS data by ensemble averaging the oscillatory data (44, 54). See SI Appendix, Supplementary Methods for additional details.

**MD Simulations.** Simulations were started from homology models built from MODELLER (80), templated from crystal structures of the pre-powerstroke state (PDB: 5N6A and 5N69) and post-rigor state (6FSA). Preparation and simulation of all systems was done using GROMACS 2022.4 (ref. 81) using a mixture of NVIDIA

- 1. A. Oldfors, Hereditary myosin myopathies. Neuromuscular Disord. 17, 355-367 (2007), 10.1016/j. nmd.2007.02.008.
- H. Tajsharghi, A. Oldfors, Myosinopathies: Pathology and mechanisms. Acta Neuropatholog. 125, 3-18 (2013), 10.1007/s00401-012-1024-2.
- B. J. Maron et al., Prevalence of hypertrophic cardiomyopathy in a general population of young adults. Circulation 92, 785-789 (1995), 10.1161/01.CIR.92.4.785.
- C. Semsarian, J. Ingles, M. S. Maron, B. J. Maron, New perspectives on the prevalence of hypertrophic cardiomyopathy. J. Am. Coll. Cardiol. 65, 1249-1254 (2015), 10.1016/j.
- M. I. Poling, C. R. Dufresne, R. L. Chamberlain, Freeman-Burian syndrome. Orphanet. J. Rare Dis. 14, 14 (2019), 10.1186/s13023-018-0984-2.
- D. I. Resnicow, J. C. Deacon, H. M. Warrick, J. A. Spudich, L. A. Leinwand, Functional diversity among a family of human skeletal muscle myosin motors. Proc. Natl. Acad. Sci. U.S.A. 107, 1053-1058 (2010), 10.1073/pnas.0913527107.
- L. J. R. Acakpo-Satchivi et al., Growth and muscle defects in mice lacking adult myosin heavy chain genes. J. Cell Biol. 139, 1219-1229 (1997), 10.1083/jcb.139.5.1219.
- D. L. Allen, L. A. Leinwand, Postnatal myosin heavy chain isoform expression in normal mice and mice null for Ilb or Ild myosin heavy chains. *Dev. Biol.* **229**, 383–395 (2001), 10.1006/dbio.2000.9974.
- C. A. Sartorius et al., Myosin heavy chains IIa and IId are functionally distinct in the mouse. J. Cell Biol. 141, 943-953 (1998), 10.1083/jcb.141.4.943.
- 10. W. Yu et al., Whole-exome sequencing reveals MYH7 p.R671C mutation in three different phenotypes of familial hypertrophic cardiomyopathy. Exp. Ther. Med. 22, 1002 (2021), 10.3892/ etm.2021.10434.
- 11. M. Toydemir et al., Mutations in embryonic myosin heavy chain (MYH3) cause Freeman-Sheldon syndrome and Sheldon-Hall syndrome. Nat. Genet. 38, 561-565 (2006), 10.1038/ng1775.
- 12. M. Veugelers et al., Mutation of perinatal myosin heavy chain associated with a carney complex variant. N. Engl. J. Med. 351, 460-469 (2004), 10.1056/NEJMoa040584.
- 13. K. Minzer-Conzetti, E. Wu, K. Vargervik, A. Slavotinek, Phenotypic variation in trismuspseudocamptodactyly syndrome caused by a recurrent MYH8 mutation. Clin. Dysmorphol. 17, 1-4 (2008), 10.1097/MCD.0b013e3282efdad8.

RTX A5000, Quadro RTX 6000, and Tesla P100 GPUs. Protein and ADP components were parameterized using CHARMM36 (ref. 82); the Karplus parameters (83) were used for inorganic phosphate, and the Allner parameters (84) for magnesium. The protein structure was solvated in a dodecahedral box of TIP3P water (85) that extended 1 nm beyond the protein in every dimension, and neutralized with 0.1 M NaCl. Each system was minimized using steepest descent until the maximum force on any atom decreased below 1,000 kJ/(mol × nm). The system was then equilibrated with all heavy atoms restrained in place at 310 K maintained by the Berendsen thermostat (86) and the Parrinello-Rahman barostat (87). Production simulations were run in the NPT ensemble at 310 K using the leapfrog integrator, Bussi-Parinello thermostat (88), and Parrinello-Rahman barostat (87). Simulation lengths varied from 500 ns-1.5  $\mu$ s, with ~70  $\mu$ s in aggregate across 90 trajectories. Trajectory analysis was conducted in Python using the library MDTraj (89). Gaussian mixture models were fitted using the implementation of the EM algorithm in scikit-learn. See SI Appendix, Supplementary Methods for additional details.

Data, Materials, and Software Availability. All study data are included in the article and/or supporting information.

ACKNOWLEDGMENTS. C.L., K.M.R., and J.A.S. were funded by NIH Grants R01 GM033289, RM1 GM131981, and HL117138 to J.A.S. C.L. was also funded by the postdoc career fund at Lawrence Livermore National Laboratory. A.K. and L.A.L. were funded by NIH Grants 5T32 HL007822 and R01 GM029090 to L.A.L. A.M. was funded by NIH F30 Fellowship 1F30HL162431-01A1. G.R.B. was funded by NSF CAREER Award MCB-1552471, NIH Grants R01 GM124007 and RF1AG067194, and Packard Fellowship for Science and Engineering from The David & Lucile Packard Foundation. The microscope was funded by NIH Grant S10RR026775 to J.A.S.

Author affiliations: <sup>a</sup>Department of Biochemistry, Stanford University School of Medicine, Stanford, CA 94305; <sup>b</sup>Stanford Cardiovascular Institute, Stanford University School of Medicine, Stanford, CA 94305; <sup>c</sup>Biosciences and Biotechnology Division, Lawrence Livermore National Laboratory, Livermore, CA 94550; dBioFrontiers Institute, University of Colorado Boulder, Boulder, CO 80309; eDepartment of Molecular, Cellular, and Developmental Biology, University of Colorado Boulder, Boulder, CO 80309; fKainomyx, Inc., Palo Alto, CA 94304; <sup>8</sup>Department of Biochemistry and Biophysics, Washington University in St. Louis, St. Louis, MO 63110; <sup>h</sup>Medical Scientist Training Program, Washington University in St. Louis, St. Louis, MO 63110; and <sup>l</sup>Department of Biochemistry and Biophysics, Perelman School of Medicine, University of Pennsylvania, Philadelphia, PA 19104

Author contributions: C.L., A.K., A.M., J.A.S., and L.A.L. designed research; C.L., A.K., A.M., and A.B. performed research; C.L., A.K., A.M., C.J.A., and G.R.B. contributed new reagents/ analytic tools; C.L., A.K., A.M., and A.B. analyzed data; G.R.B., K.M.R., J.A.S., and L.A.L. supervised; and C.L., A.K., A.M., A.B., K.M.R., and L.A.L. wrote the paper.

- R. M. Toydemir et al., Trismus-pseudocamptodactyly syndrome is caused by recurrent mutation of MYHB. Am. J. Med. Genet. Part A 140A, 2387–2393 (2006), 10.1002/ajmg.a.31495.
- J. Walklate, C. Vera, M. J. Bloemink, M. A. Geeves, L. A. Leinwand, The most prevalent freemansheldon syndrome mutations in the embryonic myosin motor share functional defects. J. Biol. Chem. 291, 10318-10331 (2016), 10.1074/jbc.M115.707489.
- 16. H. L. Sweeney, A. Houdusse, Structural and functional insights into the Myosin motor mechanism. Annu. Rev. Biophys. 39, 539-557 (2010), 10.1146/annurev.biophys.050708.133751.
- A. Weiss, L. A. Leinwand, The mammalian myosin heavy chain gene family. Ann. Rev. Cell Dev. Biol. 12, 417-439 (1996), 10.1146/annurev.cellbio.12.1.417.
- 18. S. Schiaffino, A. C. Rossi, V. Smerdu, L. A. Leinwand, C. Reggiani, Developmental myosins: Expression patterns and functional significance. Skelet. Muscle 5, 22 (2015), 10.1186/s13395-
- 19. B. J. Maron, M. S. Maron, Hypertrophic cardiomyopathy. The Lancet 381, 242-255 (2013), 10.1016/ 50140-6736(12)60397-3.
- J. A. Spertus et al., Mavacamten for treatment of symptomatic obstructive hypertrophic cardiomyopathy (EXPLORER-HCM): Health status analysis of a randomised, double-blind, placebo-controlled, phase 3 trial. *The Lancet* **397**, 2467–2475 (2021), 10.1016/S0140-6736(21)00763-7.
- 21. M. Bamshad, A. E. Van Heest, D. Pleasure, Arthrogryposis: A review and update. *J. Bone Joint Surg.* Am. 91, 40-46 (2009), 10.2106/jbjs.l.00281.
- 22. A. E. Beck et al., Genotype-phenotype relationships in Freeman-Sheldon syndrome. Am. J. Med. Genet. Part A 164, 2808-2813 (2014), 10.1002/ajmg.a.36762.
- 23. D. A. Stevenson et al., Clinical characteristics and natural history of Freeman-Sheldon Syndrome. Pediatrics 117, 754-762 (2006), 10.1542/peds.2005-1219.
- 24. A. W. Racca et al., The embryonic myosin R672C mutation that underlies Freeman-Sheldon syndrome impairs cross-bridge detachment and cycling in adult skeletal muscle. Hum. Mol. Genet. 24, 3348-3358 (2015), 10.1093/hmg/ddv084.
- K. M. Bell, A. Huang, W. A. Kronert, S. I. Bernstein, D. M. Swank, Prolonged myosin binding increases muscle stiffness in Drosophila models of Freeman-Sheldon syndrome. Biophys. J. 120, 844-854 (2021), 10.1016/j.bpj.2020.12.033.

- S. Lowey et al., Functional effects of the hypertrophic cardiomyopathy R403Q mutation are different in an alpha- or beta-myosin heavy chain backbone. J. Biol. Chem. 283, 20579-20589 (2008), 10.1074/jbc.M800554200.
- S. Lowey, V. Bretton, J. Gulick, J. Robbins, K. M. Trybus, Transgenic mouse α- and β-cardiac myosins containing the R403Q mutation show isoform-dependent transient kinetic differences. J. Biol. Chem. 288, 14780-14787 (2013), 10.1074/jbc.M113.450668.
- D. S. Rao et al., Reductions in ATPase activity, actin sliding velocity, and myofibril stability yield muscle dysfunction in Drosophila models of myosin-based Freeman-Sheldon syndrome. Mol. Biol. Cell 30, 30-41 (2019), 10.1091/mbc.E18-08-0526.
- Q. Wang, C. L. Moncman, D. A. Winkelmann, Mutations in the motor domain modulate myosin activity and myofibril organization. J. Cell Sci. 116, 4227–4238 (2003), 10.1242/jcs.00709.
- R. Srikakulam, L. Liu, D. A.Winkelmann, Unc45b forms a cytosolic complex with Hsp90 and targets the unfolded myosin motor domain. PLoS One 3, e2137 (2008), 10.1371/journal.pone.0002137.
- J. C. Deacon, M. J. Bloemink, H. Rezavandi, M. A. Geeves, L. A. Leinwand, Identification of functional differences between recombinant human alpha and beta cardiac myosin motors. *Cell Mol. Life Sci.* 69, 2261–2277 (2012), 10.1007/s00018-012-0927-3.
- C. A. Johnson et al., The ATPase cycle of human muscle myosin II isoforms: Adaptation of a single mechanochemical cycle for different physiological roles. J. Biol. Chem. 294, 14267–14278 (2019), 10.1074/jbc.RA119.009825.
- M. Kawana, J. A. Spudich, K. M. Ruppel, Hypertrophic cardiomyopathy: Mutations to mechanisms to therapies. Front. Physiol. 13, 975076 (2022), 10.3389/fphys.2022.975076.
- S. Das, P. Kumar, A. Verma, T. K. Maiti, S. J. Mathew, Myosin heavy chain mutations that cause Freeman-Sheldon syndrome lead to muscle structural and functional defects in Drosophila. *Dev. Biol.* 449, 90–98 (2019).
- 35. S. M. Mijailovich *et al.*, Modeling the actin.myosin ATPase cross-bridge cycle for skeletal and cardiac muscle myosin isoforms. *Biophys. J.* **112**, 984–996 (2017), 10.1016/j.bpj.2017.01.021.
- A. W. Racca et al., Contractility and kinetics of human fetal and human adult skeletal muscle. J. Physiol. 591, 3049–3061 (2013), 10.1113/jphysiol.2013.252650.
- R. F. Sommese et al., Molecular consequences of the R453C hypertrophic cardiomyopathy mutation on human β-cardiac myosin motor function. Proc. Natl. Acad. Sci. U.S.A. 110, 12607–12612 (2013), 10.1073/pnas.1309493110.
- T. Aksel, E. Choe Yu, S. Sutton, K. M. Ruppel, J. A. Spudich, Ensemble force changes that result from human cardiac myosin mutations and a small-molecule effector. *Cell Rep.* 11, 910-920 (2015), 10.1016/j.celrep.2015.04.006.
- S. Nag et al., Contractility parameters of human beta-cardiac myosin with the hypertrophic cardiomyopathy mutation R403Q show loss of motor function. Sci. Adv. 1, e1500511 (2015), 10.1126/sciadv.1500511.
- D. A. Winkelmann, E. Forgacs, M. T. Miller, A. M. Stock, Structural basis for drug-induced allosteric changes to human beta-cardiac myosin motor activity. *Nat. Commun.* 6, 7974 (2015), 10.1038/ 2007.4
- A. S. Adhikari et al., Early-onset hypertrophic cardiomyopathy mutations significantly increase the velocity, force, and actin-activated ATPase activity of human beta-cardiac myosin. Cell Rep. 17, 2857-2864 (2016), 10.1016/j.celrep.2016.11.040.
- C. Liu, M. Kawana, D. Song, K. M. Ruppel, J. A. Spudich, Controlling load-dependent kinetics of betacardiac myosin at the single-molecule level. *Nat. Struct. Mol. Biol.* 25, 505–514 (2018), 10.1038/ s41594-018-0069-x.
- W. Tang, W. C. Unrath, R. Desetty, C. M. Yengo, Dilated cardiomyopathy mutation in the converter domain of human cardiac myosin alters motor activity and response to omecamtiv mecarbil. *J. Biol. Chem.* 294, 17314–17325 (2019), 10.1074/jbc.RA119.010217.
- A. S. Vander Roest et al., Hypertrophic cardiomyopathy beta-cardiac myosin mutation (P710R) leads to hypercontractility by disrupting super relaxed state. Proc. Natl. Acad. Sci. U.S.A. 118, e2025030118 (2021), 10.1073/pnas.2025030118.
- C. Liu, K. M. Ruppel, J. A. Spudich, Familial Cardiomyopathies: Methods and Protocols, M. Regnier, M. Childers, Eds. (Springer US, 2024), pp. 169–189.
- J. Sung et al., Harmonic force spectroscopy measures load-dependent kinetics of individual human beta-cardiac myosin molecules. Nat. Commun. 6, 7931 (2015), 10.1038/ncomms8931.
- M. M. Morck et al., Hypertrophic cardiomyopathy mutations in the pliant and light chain-binding regions of the lever arm of human beta-cardiac myosin have divergent effects on myosin function. Elife 11, e76805 (2022), 10.7554/eLife.76805.
- R. F. Siemankowski, H. D. White, Kinetics of the interaction between actin, ADP, and cardiac myosin-S1. J. Biol. Chem. 259, 5045–5053 (1984).
- R. F. Siemankowski, M. O. Wiseman, H. D. White, ADP dissociation from actomyosin subfragment 1 is sufficiently slow to limit the unloaded shortening velocity in vertebrate muscle. *Proc. Natl. Acad. Sci.* U.S.A. 82, 658–662 (1985), 10.1073/pnas.82.3.658.
- C. Veigel, J. E. Molloy, S. Schmitz, J. Kendrick-Jones, Load-dependent kinetics of force production by smooth muscle myosin measured with optical tweezers. *Nat. Cell Biol.* 5, 980-986 (2003), 10.1038/ pcb1020
- M. Nyitrai et al., What limits the velocity of fast-skeletal muscle contraction in mammals? J. Mol. Biol. 355, 432–442 (2006), 10.1016/j.jmb.2005.10.063.
- M. J. Greenberg, H. Shuman, E. M. Ostap, Inherent force-dependent properties of beta-cardiac myosin contribute to the force-velocity relationship of cardiac muscle. *Biophys. J.* 107, L41–L44 (2014), 10.1016/j.bpj.2014.11.005.
- M. S. Woody et al., Positive cardiac inotrope omecamtiv mecarbil activates muscle despite suppressing the myosin working stroke. Nat. Commun. 9, 3838 (2018), 10.1038/s41467-018-06193-2.
- C. Veigel et al., The motor protein myosin-I produces its working stroke in two steps. Nature 398, 530-533 (1999), 10.1038/19104.
- M. S. Woody, D. A. Winkelmann, M. Capitanio, E. M. Ostap, Y. E. Goldman, Single molecule mechanics resolves the earliest events in force generation by cardiac myosin. *Elife* 8, e49266 (2019), 10.7554/eLife.49266.

- R. K. Brizendine et al., A mixed-kinetic model describes unloaded velocities of smooth, skeletal, and cardiac muscle myosin filaments in vitro. Sci. Adv. 3, eaao2267 (2017), 10.1126/sciadv.aao2267.
- T. Q. Uyeda, S. J. Kron, J. A. Spudich, Myosin step size. Estimation from slow sliding movement of actin over low densities of heavy meromyosin. J. Mol. Biol. 214, 699-710 (1990), 10.1016/0022-2836(90)90287-V.
- S. Walcott, D. M. Warshaw, E. P. Debold, Mechanical coupling between myosin molecules causes differences between ensemble and single-molecule measurements. *Biophys. J.* 103, 501–510 (2012), 10.1016/j.bpj.2012.06.031.
- K. M. Hart, C. M. Ho, S. Dutta, M. L. Gross, G. R. Bowman, Modelling proteins' hidden conformations to predict antibiotic resistance. *Nat. Commun.* 7, 12965 (2016), 10.1038/ncomms12965.
- J. R. Porter, A. Meller, M. I. Zimmerman, M. J. Greenberg, G. R. Bowman, Conformational distributions of isolated myosin motor domains encode their mechanochemical properties. *Elife* 9, e55132 (2020), 10.7554/eLife.55132.
- A. Meller et al., Drug specificity and affinity are encoded in the probability of cryptic pocket opening in myosin motor domains. Elife 12, e83602 (2023), 10.7554/eLife.83602.
- L. A. Lee et al., Functional divergence of the sarcomeric myosin, MYH7b, supports species-specific biological roles. J. Biol. Chem. 299, 102657 (2023), 10.1016/j.jbc.2022.102657.
- M. D. Ward et al., Deep learning the structural determinants of protein biochemical properties by comparing structural ensembles with DiffNets. Nat. Commun. 12, 3023 (2021), 10.1038/s41467-021-23246-1.
- B. Takacs et al., Myosin cleft closure determines the energetics of the actomyosin interaction. FASEB J. 25, 111-121 (2011).
- M. Kawana, S. S. Sarkar, S. Sutton, K. M. Ruppel, J. A. Spudich, Biophysical properties of human β-cardiac myosin with converter mutations that cause hypertrophic cardiomyopathy. Sci. Adv. 3, e1601959 (2017). 10.1126/sciady.1601959.
- S. S. Sarkar et al., The hypertrophic cardiomyopathy mutations R403Q and R663H increase the number of myosin heads available to interact with actin. Sci. Adv. 6, eaax0069 (2020), 10.1126/ sciady.aax0069.
- A. Snoberger et al., Myosin with hypertrophic cardiac mutation R712L has a decreased working stroke which is rescued by omecamtiv mecarbil. Elife 10, e63691 (2021), 10.7554/eLife.63691
- S. Nag et al., The myosin mesa and the basis of hypercontractility caused by hypertrophic cardiomyopathy mutations. Nat. Struct. Mol. Biol. 24, 525-533 (2017), 10.1038/nsmb.3408.
- L. Alamo et al., Effects of myosin variants on interacting-heads motif explain distinct hypertrophic and dilated cardiomyopathy phenotypes. Elife 6, e24634 (2017), 10.7554/eLife.24634.
- J. R. Teerlink et al., Cardiac myosin activation with omecamtiv mecarbil in systolic heart failure. N. Engl. J. Med. 384, 105–116 (2020), 10.1056/NEJMoa2025797.
- B. J. Maron, J. J. Doerer, T. S. Haas, D. M. Tierney, F. O. Mueller, Sudden deaths in young competitive athletes: Analysis of 1866 deaths in the United States, 1980-2006. Circulation 119, 1085-1092 (2009), 10.1161/CIRCULATIONAHA.108.804617.
- M. Regnier, A. J. Rivera, Y. Chen, P. B. Chase, 2-deoxy-ATP enhances contractility of rat cardiac muscle. Circ. Res. 86, 1211–1217 (2000), 10.1161/01.res.86.12.1211.
- M. Kovács, J. Tóth, C. Hetényi, A. Málnási-Csizmadia, J. R. Sellers, Mechanism of Blebbistatin Inhibition of Myosin II. J. Biol. Chem. 279, 35557–35563 (2004), 10.1074/jbc.M405319200.
- J. A. Rohde, O. Roopnarine, D. D. Thomas, J. M. Muretta, Mavacamten stabilizes an autoinhibited state of two-headed cardiac myosin. *Proc. Natl. Acad. Sci. U.S.A.* 115, E7486–E7494 (2018), 10.1073/pnas.1720342115.
- R. L. Anderson et al., Deciphering the super relaxed state of human beta-cardiac myosin and the mode of action of mavacamten from myosin molecules to muscle fibers. Proc. Natl. Acad. Sci. U.S.A. 115, E8143–E8152 (2018), 10.1073/pnas.1809540115.
- J. Huang, S. S. Nagy, A. Koide, R. S. Rock, S. A. Koide, A peptide tag system for facile purification and single-molecule immobilization. *Biochemistry* 48, 11834–11836 (2009), 10.1021/bi901756n.
- E. M. De La Cruz, E. M. Ostap, Kinetic and equilibrium analysis of the myosin ATPase. Methods Enzymol. 455, 157-192 (2009), 10.1016/S0076-6879(08)04206-7.
- S. J. Kron, J. A. Spudich, Fluorescent actin filaments move on myosin fixed to a glass surface. Proc. Natl. Acad. Sci. U.S.A. 83, 6272–6276 (1986), 10.1073/pnas.83.17.6272.
- J. Sung, K. I. Mortensen, J. A. Spudich, H. Flyvbjerg, How to measure load-dependent kinetics of individual motor molecules without a force-clamp. *Methods Enzymol.* 582, 1–29 (2017), 10.1016/ bs.mie.2016.08.002.
- A. Sali, T. L. Blundell, Comparative protein modelling by satisfaction of spatial restraints. J. Mol. Biol. 234, 779–815 (1993).
- M. J. Abraham et al., GROMACS: High performance molecular simulations through multilevel parallelism from laptops to supercomputers. SoftwareX 1, 19–25 (2015), 10.1016/j. softx.2015.06.001.
- J. Huang et al., CHARMM36m: An improved force field for folded and intrinsically disordered proteins. Nat. Methods 14, 71–73 (2017), 10.1038/nmeth.4067.
- M. Cecchini, M. Alexeev Y Fau-Karplus, M. Karplus, Pi release from myosin: A simulation analysis of possible pathways. Structure 18, 458–470 (2010).
- O. Allnér, L. Nilsson, A. Villa, Magnesium ion-water coordination and exchange in biomolecular simulations. J. Chem. Theory Comput. 8, 1493–1502 (2012).
- W. L. Jorgensen, J. Chandrasekhar, J. D. Madura, R. W. Impey, M. L. Klein, Comparison of simple potential functions for simulating liquid water. J. Chem. Phys. 79, 926-935 (1983), 10.1063/1.445869.
- H. J. C. Berendsen, J. P. M. Postma, W. F. van Gunsteren, A. DiNola, J. R. Haak, Molecular dynamics with coupling to an external bath. J. Chem. Phys. 81, 3684-3690 (1984), 10.1063/1.448118.
- M. Parrinello, A. Rahman, Polymorphic transitions in single crystals: A new molecular dynamics method. J. Appl. Phys. 52, 7182–7190 (1981), 10.1063/1.328693.
- G. Bussi, D. Donadio, M. Parrinello, Canonical sampling through velocity rescaling. J. Chem. Phys 126, 014101 (2007), 10.1063/1.2408420.
- R.T. McGibbon et al., MDTraj: A modern open library for the analysis of molecular dynamics trajectories. Biophys. J. 109, 1528–1532 (2015), 10.1016/j.bpj.2015.08.015.